

MATERIALS SCIENCE

Mass production of 2D materials by intermediate-assisted grinding exfoliation

Chi Zhang^{1,†}, Junyang Tan^{1,†}, Yikun Pan¹, Xingke Cai¹, Xiaolong Zou¹,
Hui-Ming Cheng^{1,2,3,*} and Bilu Liu^{1,*}

ABSTRACT

The scalable and high-efficiency production of 2D materials is a prerequisite to their commercial use. Currently, only graphene and graphene oxide can be produced on a ton scale, and the inability to produce other 2D materials on such a large scale hinders their technological applications. Here we report a grinding exfoliation method that uses micro-particles as force intermediates to resolve applied compressive forces into a multitude of small shear forces, inducing the highly efficient exfoliation of layer materials. The method, referred to as intermediate-assisted grinding exfoliation (iMAGE), can be used for the large-scale production of many 2D materials. As an example, we have exfoliated bulk h-BN into 2D h-BN with large flake sizes, high quality and structural integrity, with a high exfoliation yield of 67%, a high production rate of 0.3 g h^{-1} and a low energy consumption of $3.01 \times 10^6 \text{ J g}^{-1}$. The production rate and energy consumption are one to two orders of magnitude better than previous results. Besides h-BN, this iMAGE technology has been used to exfoliate various layer materials such as graphite, black phosphorus, transition metal dichalcogenides, and metal oxides, proving its universality. Molybdenite concentrate, a natural low-cost and abundant mineral, was used as a demo for the large-scale exfoliation production of 2D MoS₂ flakes. Our work indicates the huge potential of the iMAGE method to produce large amounts of various 2D materials, which paves the way for their commercial application.

Keywords: 2D materials, hexagonal boron nitrides, transition metal dichalcogenides, intermediary-assisted grinding exfoliation, mass production

INTRODUCTION

The large number of 2D materials, including graphene, hexagonal boron nitride (h-BN), transition metal dichalcogenides (TMDCs) like MoS₂ and WSe₂, metal oxides (M_xO_y), black phosphorene (b-P), etc, provide a wide range of properties and numerous potential applications [1–7], but achieving these requires scalable production. Bottom-up strategies like chemical vapor deposition (CVD) and chemical synthesis have been extensively explored but only small quantities have been produced so far [8,9]. For example, the highest production of CVD-grown graphene is on the order of 1 000 000 m² per year, which is equal to ~0.77 kg, while for other CVD-grown 2D materials it is much less [10,11]. Moreover, the high growth temperatures (450–1100°C) and time-consuming transfer processes usually needed for CVD-grown

2D materials result in high cost and a low production rate [11]. As for the chemical synthesis strategy, solvothermal treatment has been used to synthesize different kinds of 2D materials including not only TMDCs [12] but also M_xO_y [13] and b-P [14], which are hard to be synthesized by CVD; however, the quantity is still small. Another strategy for the preparation of 2D materials is top-down exfoliation, which involves exfoliating bulk layer materials to a monolayer or few-layer flakes [3,7,15–18]. Micromechanical exfoliation using Scotch[®] tape can produce 2D materials of the highest quality, but in negligible amounts [19]. Although there are other techniques to exfoliate layer materials that can be scaled up, they are only suitable for specific materials and/or require harsh conditions [2,3,18,20]. So far, only graphene and graphene oxide can be prepared at the ton level and the

¹Shenzhen Geim Graphene Center, Tsinghua-Berkeley Shenzhen Institute & Tsinghua Shenzhen International Graduate School, Tsinghua University, Shenzhen 518055, China; ²Shenyang National Laboratory for Materials Science, Institute of Metal Research, Chinese Academy of Sciences, Shenyang 110016, China and ³Advanced Technology Institute, University of Surrey, Guildford GU2 7XH, UK

*Corresponding authors. E-mails: hmcheng@sz.tsinghua.edu.cn; bilu.liu@sz.tsinghua.edu.cn

[†]Equally contributed to this work.

Received 21 August 2019; Revised 17 September 2019; Accepted 17 September 2019

difficulties in preparing other 2D materials in such a large quantity has significantly hindered their commercialization [11]. Among the current exfoliation techniques, ball milling [17,21] and liquid phase exfoliation [22,23], which use shear forces to induce slipping between adjacent layers, are promising for the scalable production of 2D materials other than graphene, such as h-BN and MoS₂. However, ball milling usually needs a long time (e.g. 20 h) to achieve high-yield (85%) exfoliation and the 2D materials obtained are small (~100 nm in lateral size) due to the large impact force of the irregularly moving hard balls [17]. On the other hand, liquid phase exfoliation can produce 2D materials of high quality on a large scale [22,24,25], but has a very low yield (<3%). In addition, the materials produced have low concentrations (<0.1 mg mL⁻¹) [24,25] in organic/surfactant solvents, and may need additional condensation and/or separation to concentrate them for use. It is obvious that both ball milling and liquid phase exfoliation still face many challenges for the scalable production of good-quality 2D materials. An ideal exfoliation method for the commercial scalable production of 2D materials should meet the following requirements. First, the exfoliated products should have a large lateral size and high quality with good structural integrity, because size and quality are the two main parameters that influence the material's properties. Second, the method should be efficient, with a high exfoliation yield and a high production rate. Third, the process should be cheap, green and requires a low energy input, in particular when considering large-scale production. Fourth, it would be ideal if the method could be universal for the exfoliation of different layer materials. Unfortunately, such a method is still unavailable.

Note that layer materials like graphite and MoS₂ possess low coefficients of friction and have been used as solid lubricants in industry for more than half a century [26]. They can buffer a large compressive force (F_c) between rolls by releasing a frictional force (F_f), transferred from F_c , through slip between adjacent layers in their structure [27]. By increasing F_c , F_f increases accordingly and eventually leads to the failure of the lubricant, which means irreversible sliding of the layers, i.e. exfoliation of these layer lubricants into thin 2D flakes. In principle, such a process would not have a big impact on the quality of the exfoliated material, because F_f is parallel to planes of the material and no additional chemicals are involved during the process. Note that a large force is not needed to exfoliate layer materials because of the weak van der Waals interactions between their layers, as revealed by experimental measurements [28] and

theoretical calculations [29]. For example, for a graphite flake with a lateral size of 10 μm , slip between layers happens at a small shear force of 3.9 μN [28]. In comparison, the shear force provided by milling rolls is on the order of tens to hundreds of newtons, over six to eight orders of magnitude higher than the force needed to exfoliate graphite. Therefore, the critical factor in increasing the exfoliation efficiency is how to effectively produce a frictional force (F_f) on a layer material.

Based on the above analysis, we have developed an exfoliation technology that we call intermediate-assisted grinding exfoliation (iMAGE) that essentially meets these requirements. The key to our method is to use intermediate materials that increase the coefficient of friction of the mixture and effectively apply sliding frictional forces to the layer material, resulting in a dramatically increased exfoliation efficiency. Considering the case of 2D h-BN, the production rate and energy consumption can reach 0.3 g h⁻¹ and 3.01 $\times 10^6$ J g⁻¹, respectively, both of which are one to two orders of magnitude better than previous results. The resulting exfoliated 2D h-BN flakes have an average thickness of 4 nm and an average lateral size of 1.2 μm . This iMAGE method has been extended to a series of layer materials with different properties, including graphite, b-P, TMDCs, and metal oxides. To further demonstrate this scaling up, molybdenite concentrate, a naturally existing cheap and earth-abundant mineral, has been used for the large-scale exfoliation production of 2D MoS₂, making the commercial production and application of 2D MoS₂ feasible.

RESULTS AND DISCUSSION

Figure 1a shows a schematic of the iMAGE method, and the experimental details are described in the 'Methods' section. In short, the intermediates convert a macroscopic compressive force F_c into microscopic forces f_i on a layer material, so that $F_c = \sum_{i=1}^n f_i$, where n is the number of microscopic forces in each box enclosed by the dashed line. The microscopic forces on each layer in the box must balance in the pressure direction, namely $F_c = \sum_{i=1}^n f_i = \sum_{i=1}^n f'_i = F'_c$, where f'_i is a microscopic force from the balancing force of the bottom F'_c . Under grinding, the rotation of the platter at the bottom of the instrument induces slipping between the layer material and the force intermediate, and f_i is converted into a sliding frictional force f_{fi} , where $f_{fi} = \mu f_i$, where μ is the sliding coefficient of friction between the intermediate and the layer material (Fig. 1b). When the shear friction force $f_{fi} > bE_e$, where b and E_e are the width and exfoliation energy of the layer material, the layers will slip and become exfoliated

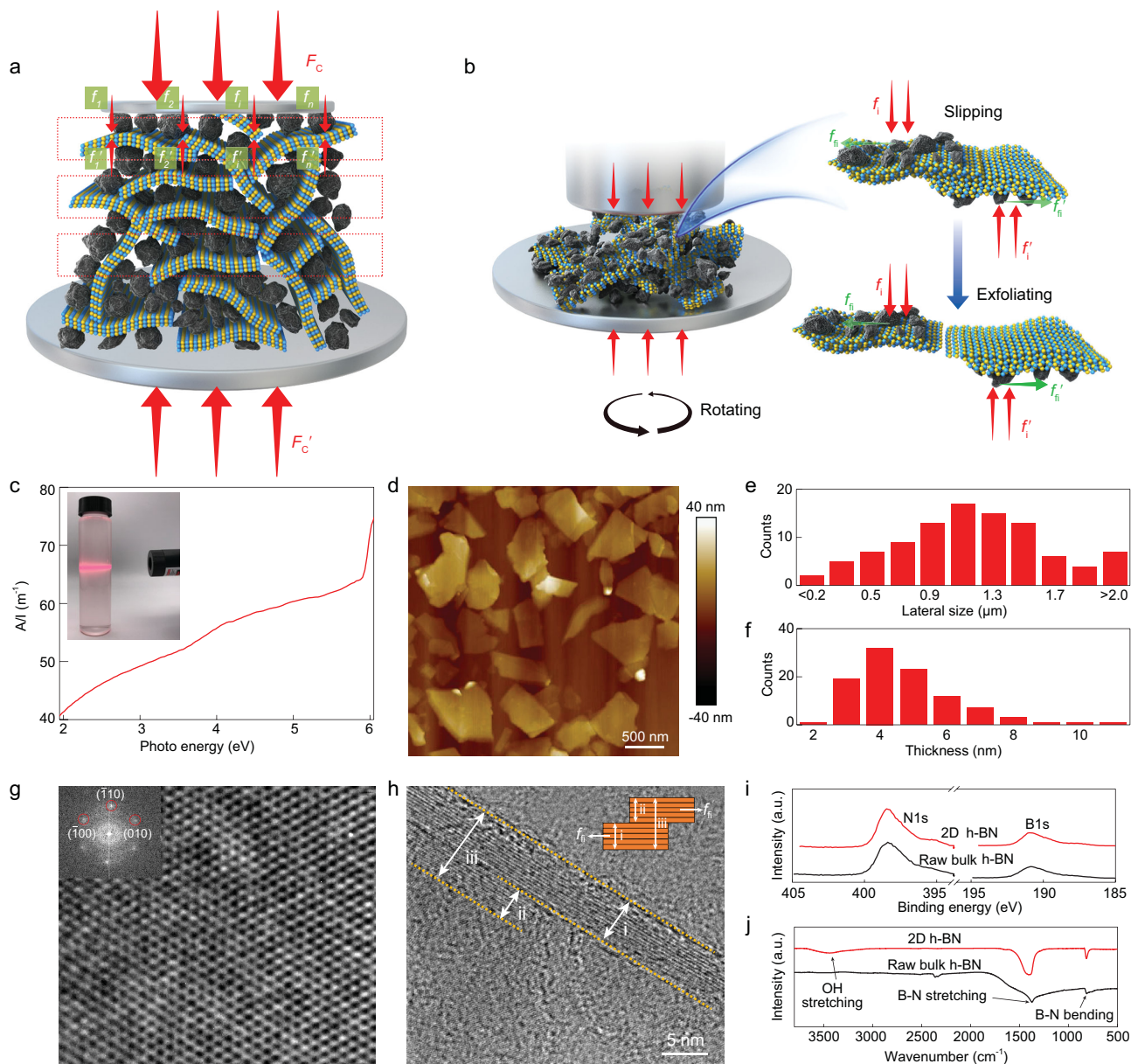


Figure 1. Exfoliation mechanism of the iMAGE method and characterization of as-prepared 2D h-BN. (a) Schematic of the decomposition of the macroscopic compressive forces F_C and F_C' into much smaller microscopic forces f_i and f_i' that were loaded onto the layer materials by force intermediates. (b) Exfoliation mechanism of layer materials. f_i and f_i' transfer to sliding frictional forces f_{ii} and f_{ii}' under the relative slipping of the intermediates and layer materials due to the rotation of the bottom container. When $f_{ii} > bE_c$, exfoliation of the layer material occurs. Note that here b is the width of the layered materials, and the unit of bE_c is $(\text{m}) \cdot (\text{J} \cdot \text{m}^{-2}) = \text{N}$. (c) A UV-vis-NIR absorption spectrum of exfoliated 2D h-BN dispersed in DI water. Inset shows the Tyndall effect of the dispersion. (d–f) AFM image, statistical analysis of the lateral size and thickness of 2D h-BN. (g) An HRTEM image of the in-plane structure of exfoliated 2D h-BN and its FFT pattern (inset). (h) Edge structure of the exfoliated 2D h-BN, showing that region ii separates from region iii. Inset in (h) is an illustration of the sliding and exfoliation process. (i, j) XPS and FTIR spectra of the raw h-BN and exfoliated 2D h-BN.

(Fig. S1), analogous to the failure of the solid lubricants discussed above [28].

The effectiveness of the iMAGE method was evaluated by exfoliating h-BN because its exfoliation into a few layers (thickness < 5 nm) with a high yield and high quality is challenging [17,20,21,30,31]. In a typical experiment, bulk h-BN was ground with silicon carbide (SiC) particles, which were used as the

force intermediate, using an apparatus that can provide a compressive force on the order of hundreds of newtons with a rotation speed of 200 rpm (see the section entitled ‘Methods’ and Fig. S2). After grinding, the mixture contained exfoliated and unexfoliated h-BN, and the SiC intermediate. To isolate the exfoliated 2D h-BN, the mixture was dispersed in deionized (DI) water; after standing for 8 h, a green

sediment containing SiC and unexfoliated h-BN was seen, and the supernatant was milky white (Fig. S3). The observation of a clear Tyndall effect in the supernatant indicates the colloidal state of the exfoliated 2D h-BN in DI water (Fig. 1c). UV-vis-NIR optical absorption measurements of this supernatant show an optical bandgap of 5.8 eV based on the plot of $(Ah\nu)^2$ versus photon energy $h\nu$ (A stands for absorbance), indicating that the dispersed material is high-quality h-BN with its original structure, which is confirmed by its white color (Figs 1c and S3) [32]. To verify the production of exfoliated 2D h-BN, SiC particles and bulk h-BN were independently added to DI water, and both precipitated completely within 5 min (Fig. S4) with a clear supernatant. These results confirm the separation of 2D h-BN from the mixture by simply dispersing it in water and standing. Previous studies show that nanomaterials can be dispersed in solvents when they have a surface energy that matches that of the solvent. The surface energy of 2D h-BN is in the range 44–66 mJ m^{-2} [16] and that of DI water is 72 mJ m^{-2} so this is not the best match, but it is the most commonly used moderate solvent and has an acceptable solvability for 2D h-BN. In contrast, SiC and h-BN particles cannot be stabilized in DI water due to a mismatch of surface energy, and quickly precipitate because they have densities larger than the solvent, i.e. 3.2 g cm^{-3} for SiC and 2.3 g cm^{-3} for h-BN, while that for DI water is only 1.0 g cm^{-3} .

The lateral size, thickness, and quality of the 2D h-BN produced are important parameters for evaluation of this iMAGE technique (Figs 1d and S5). Statistical analysis of the products by atomic force microscopy (AFM) indicates that the 2D h-BN has an average lateral size of 1.2 μm (Fig. 1e), consistent with the dynamic light scattering (DLS) results (Fig. S6), and an average thickness of 4 nm (Fig. 1f). To the best of our knowledge, this average lateral size is the largest so far obtained for top-down exfoliated 2D h-BN (Table S1). In addition, the results from high-resolution transmission electron microscopy (HRTEM) observations and fast Fourier transformation (FFT) analysis show high-quality 2D h-BN sheets (Fig. 1g) without noticeable defects in the planes and along the edges. The crystalline quality of the 2D h-BN is comparable with that of samples prepared by liquid phase exfoliation [22] and is superior to that of the samples obtained from intercalation [33] and ball milling [21], which have many structural defects and functional groups. The clear lattice fringes on the edge indicate negligible damage to the layer structure when transforming bulk h-BN into thin 2D sheets (Figs 1h and S7). The large size and high quality of the obtained 2D h-BN must result from the unique exfoliation mode in

the iMAGE process. During exfoliation, the SiC particles contact and interact with the top layers of bulk h-BN, causing them to slip with negligible damage to their in-plane structure. Figure 1h shows a 10-layer h-BN step (region ii) slipping from 25-layer h-BN (region iii), similar to previous *in situ* TEM studies of the exfoliation of MoS_2 , where the sliding of 2D sheets from the mother MoS_2 has been clearly identified under a shear force [34], consistent with the exfoliation mechanism proposed above.

Various spectroscopic characterization techniques confirm that the iMAGE-produced 2D h-BN has good quality with no noticeable functional groups (Fig. 1i, j; Supplementary Information, Section 1.1, Figs S7 and S8). For example, X-ray photoemission spectroscopy (XPS) of 2D h-BN shows two major peaks at 190.2 and 398.2 eV for B1s and N1s, the same as those for bulk h-BN, without any functional group-related peaks (Fig. 1i). Fourier transformation infrared (FTIR) analysis directly proves the absence of functional groups on the iMAGE-produced 2D h-BN (Fig. 1j). We note that the shapes of FTIR peaks for exfoliated 2D h-BN and bulk h-BN are different. This could be attributed to the reduced size and thickness after exfoliation. Compared to the lateral size of the exfoliated h-BN (1.2 μm), the size of the bulk h-BN (30 μm) is closer to the wavelength of infrared light in FTIR (0.2–20 μm), which would lead to much stronger light scattering and cause baseline drift as well as peak broadening in bulk h-BN (Figs 1j and S8). In addition, after exfoliation, due to the significantly reduced thickness, the B–N stretching and bending could be excited more easily, which will sharpen the FTIR peaks of the exfoliated h-BN [35]. Moreover, the Raman peak position of the B–N vibration mode (E_{2g}) for the exfoliated 2D h-BN is 1366 cm^{-1} , the same as that for bulk h-BN, also indicating negligible change to the intrinsic bonding (Fig. S7). These results are expected because iMAGE is a purely mechanical process in which no chemical reactions take place.

Based on the principle of friction force-induced sliding and exfoliation in the iMAGE technique, exfoliation occurs when $f_{\text{fi}} > bE_e$. Therefore, the parameters that influence f_{fi} , b and E_e will affect the exfoliation efficiency. It is clear that the size of the force intermediate will affect the exfoliation yield. For the bulk h-BN with a 30 μm particle size used in this study, the frictional force f_{fi} needs to be larger than 13.8 μN assuming that the exfoliation energies E_e for h-BN and graphite are identical, i.e. 0.46 J m^{-2} [28,29]. We calculated the frictional force on h-BN applied by each SiC particle (Supplementary Information, Section 1.4 and Table S2), demonstrating that only particles larger than 73 μm can exert an

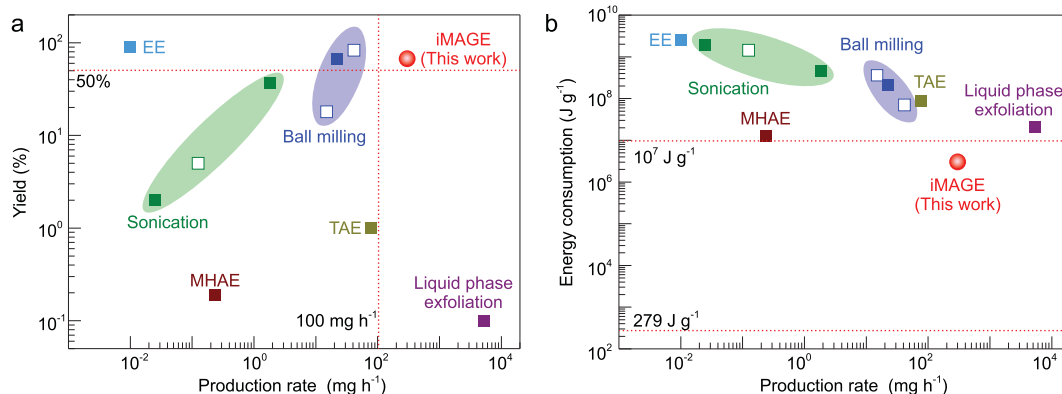


Figure 2. High-efficiency exfoliation of 2D h-BN by the iMAGE technique. (a) Exfoliation yield versus production rate and (b) energy consumption versus production rate, for different exfoliation methods, including ball milling, sonication, liquid phase exfoliation, electrochemical exfoliation (EE), turbulence-assisted exfoliation (TAE), molten hydroxide-assisted exfoliation (MHAE), and this method (iMAGE). Note that the solid (or empty) boxes stand for non-functionalized (or functionalized) 2D h-BN materials.

average frictional force greater than 13.8 μN . This result shows that the sizes of the raw bulk materials and the intermediate particles should be matched to obtain a high exfoliation yield. An exfoliation yield of 67% is confirmed by both direct measurements of the weight of 2D h-BN and UV-vis absorption measurements (Supplementary Information, Section 1.2, Section 1.3, Figs S9 and S10), which is one of the highest reported values for the exfoliation of pristine 2D h-BN (Supplementary Table S1), and it was achieved in 270 min. Such fast high-yield exfoliation can be understood when compared to the ball milling method (Supplementary Table S3). In the iMAGE process, the weight of the intermediates was almost an order of magnitude lower than that of the balls used in ball milling [31]; however, the number of particles is four orders of magnitude higher and the surface area is doubled, both of which facilitate the effective transfer of frictional force to the layer material, leading to a shorter exfoliation time with a much higher yield.

In addition to the exfoliation yield, production rate and energy consumption are the other two important parameters to be considered for the commercialization of the iMAGE method. Typically, when 2 g of bulk h-BN was used, the production rate of 2D h-BN could reach 0.3 g h⁻¹, which is around 10 times that of a typical ball milling method for preparing amino-functionalized small 2D h-BN sheets [17]. This rate is the highest value reported for h-BN production to date (Supplementary Table S1). The method achieves both a high yield and a high production rate (Fig. 2a), and this is the first time that a 2D material other than graphene has been produced with a yield of more than 50% and a production rate of over 0.1 g h⁻¹. The annual production capability of 2D h-BN is expected to exceed 10 tons

by the iMAGE technology (Supplementary Information, Section 1.4). For comparison, electrochemical intercalation [18] and liquid phase exfoliation [22] can achieve only a high yield or a high production rate, while ball milling may produce functionalized 2D materials with a high yield but a medium production rate. In addition, our method requires an energy consumption of only $3.01 \times 10^6 \text{ J g}^{-1}$ to exfoliate bulk h-BN, which is at least a tenth of that of other methods (Fig. 2b and Supplementary Table S1). According to theoretical calculations, the minimum energy required to exfoliate 1 g h-BN is 279 J (Supplementary Table S4), three orders of magnitude lower than the value for our method, demonstrating that there is still much room for improvement. In short, the iMAGE method requires a low energy to produce 2D materials because of its efficient transfer of force and energy to the layer materials, while the production rate is among the highest, making it a practical method for the commercial scalable production of 2D h-BN.

Besides SiC, several other hard micro-particles, such as Mo₂C and cheap sea sand, were also used as intermediate materials to transmit the sliding frictional force onto bulk h-BN, and lead to the efficient exfoliation of h-BN, demonstrating that the economical production of 2D materials could be realized by using cheap intermediates. The process would also be valuable for the one-step fabrication of 2D material-based composites in which an intermediate is a functional component in the composite material.

In addition to h-BN, we have extended the method to a series of layer materials with a wide range of properties. Not only air-stable metallic graphite, *n*-type semiconducting Bi₂Te₃ and MoS₂, and insulating mica, but also air-sensitive *p*-type

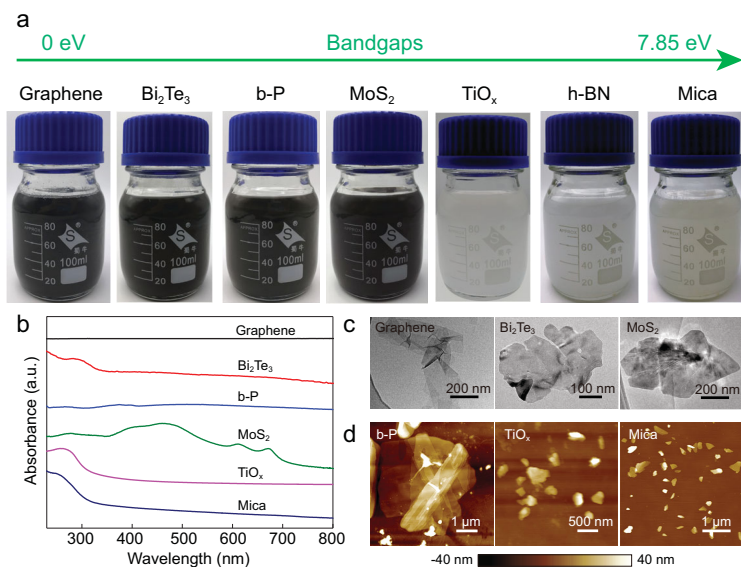


Figure 3. Extension of the iMAGE technique to exfoliate other layer materials. (a) Digital images, (b) UV-vis-NIR absorption spectra, and (c, d) TEM and AFM images of as-prepared 2D materials including metallic graphene, semiconducting Bi_2Te_3 , b-P, MoS_2 and TiO_x , as well as insulating mica, confirming their 2D features.

semiconducting b-P were exfoliated into few layers (Figs 3a, S12, S13 and S14). UV-vis-NIR absorption (Fig. 3b) shows the wavelength-independent absorbance for the above materials in the visible light range. For graphene, the curve is similar to the Scotch[®] tape-exfoliated [36] and CVD-grown materials [37], but different from graphene oxide [4]. For as-exfoliated 2D TiO_x , mica and Bi_2Te_3 , the characteristic absorption bands are almost at the same positions as those of the raw bulk materials (Fig. S12 and previous reports [38,39]). In addition, for Bi_2Te_3 the appearance of a prominent absorption peak at 265 nm reveals the production of few-layer 2D Bi_2Te_3 [40]. These results confirm that the iMAGE-produced 2D materials have good structural integrity rather than having been functionalized.

Regarding the size and thickness of the exfoliated 2D materials, taking MoS_2 as an example (Fig. S13), AFM measurements show that the exfoliated flakes have an average thickness of 10 nm and an average lateral size of 600 nm. The size of bulk raw MoS_2 used for this exfoliation was less than 2 μm , which is small. By using MoS_2 crystals with a larger size and optimizing the iMAGE process we could, in principle, obtain larger flakes. Raman analysis shows a redshift in the A_{1g} phonon mode of 2D MoS_2 compared to bulk MoS_2 , which is attributed to the lower interlayer van der Waals force after exfoliation [16]. The high quality of these exfoliated 2D MoS_2 is confirmed by HRTEM examination and UV-vis-NIR absorption with characteristic absorp-

tion peaks at 672 and 610 nm (Fig. S13) [41,42]. The other layer materials (Figs 3c, d and S12) were exfoliated into a few layers with average thicknesses less than 10 nm and lateral sizes of 400–1000 nm under non-optimized conditions. Air-sensitive layer materials, such as b-P, have also been exfoliated by the iMAGE process in an argon- or nitrogen-filled glove box. The thickness of exfoliated 2D b-P is around 2–4 nm, as revealed by AFM characterization (Fig. 3d). The UV-vis-NIR absorption spectrum shows a broad absorption peak around 520 nm (Fig. S14) as the wavelength range used has a much higher energy than the bandgap of b-P, which is similar to the previous reported results [43]. Raman spectroscopy shows that the A_g^1/A_g^2 ratios of exfoliated b-P and the bulk material were 0.88 and 0.68 (Fig. S14), respectively, which are both larger than the oxidation criterion value (0.6), indicating that the 2D b-P flakes obtained were not oxidized after iMAGE exfoliation [44].

As a step further, we used iMAGE to exfoliate abundant and cheap natural layer minerals to produce large quantities of 2D materials, e.g. MoS_2 . The industrial production of MoS_2 ore follows the following procedure. 1) Finding a Mo-rich mine where the Mo concentration is higher than 0.1 wt% (Fig. 4a). 2) Drilling and blasting to obtain an ore with a size of a few meters (Fig. 4b). 3) Crushing the ore to a size of 10–20 μm . 4) Floating the ore to obtain a Mo-enriched molybdenite concentrate where Mo > 45 wt% (Fig. 4c). This concentrate can then be used for the iMAGE exfoliation to prepare 2D MoS_2 . Note that in the current molybdenum industry, the molybdenite concentrate is the flotation product of a natural ore and the precursor to industrial-grade MoS_2 . Because of its earlier production in the manufacturing processes, molybdenite concentrate has a much lower price ($\sim \$2.6 \times 10^2/\text{t}$) than other molybdenum sources, e.g. 2.36% of the price of industrial-grade MoS_2 ($\sim \$1.1 \times 10^4/\text{t}$) and only 0.04% of the high-purity MoS_2 chemical from several vendors ($\sim \$7.0 \times 10^5/\text{t}$). The natural layer structure and low price suggest that molybdenite concentrate could be an ideal choice of starting material for the scalable exfoliation of 2D MoS_2 .

Scanning electron microscopy (SEM) inspection shows that a bulk molybdenite concentrate does not have a well-defined layer structure because the main part is cubic particles with some layer-structured material on its surface (Fig. S15). By using the iMAGE method we prepared 60 L of few-layer molybdenite dispersed in water (0.25 mg mL^{-1}) in less than 270 min (Fig. 4d). The concentrations of 2D materials could be further increased, e.g. to >5 mg mL^{-1} , by using suitable solvents or adding surfactants in water. AFM and TEM show that the lateral size

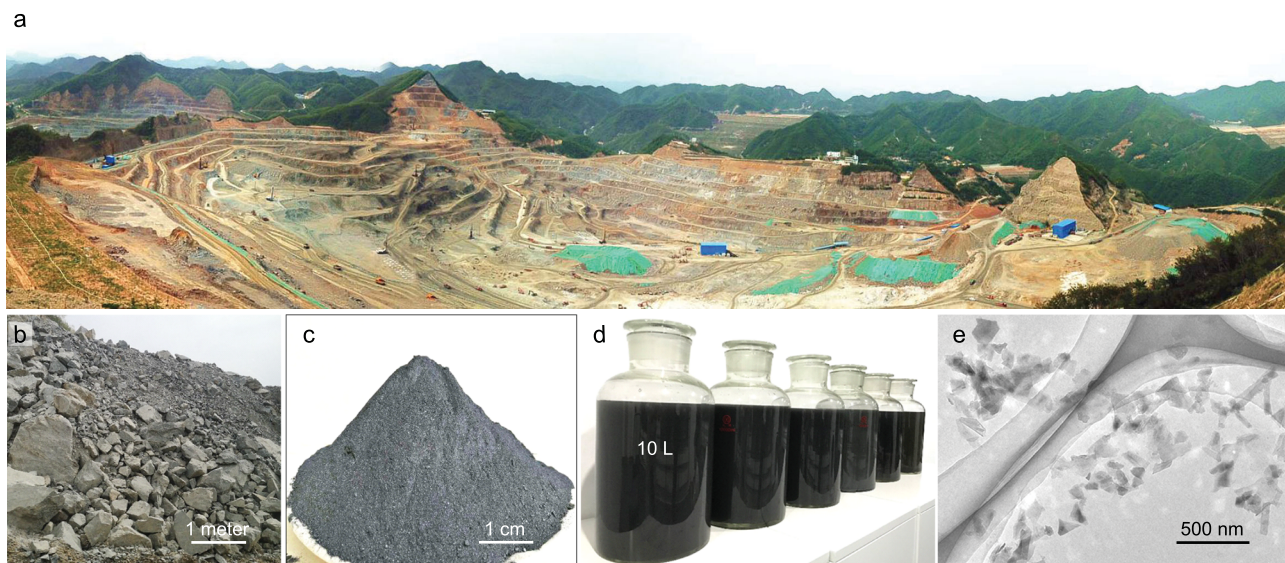


Figure 4. Large-scale production of 2D MoS₂ from a cheap molybdenite concentrate. (a) Bird's eye view of the Sandaozhuang open-pit mine in Luoyang, China. The size of the mine is around 1.5 × 1.5 km, and the depth is around 400 m. (b–d) Digital images of ores, molybdenite concentrates, and 60 L of as-prepared 2D MoS₂ aqueous dispersions with a concentration of 0.25 mg mL⁻¹, respectively. (e) A TEM image of the exfoliated 2D MoS₂.

of the material was 200–300 nm (Fig. 4e). UV–vis–NIR absorption and Raman spectroscopy results confirm the high quality of the MoS₂ exfoliated from molybdenite concentrate (Fig. S15), and are the same as those obtained from MoS₂ exfoliated from MoS₂ chemicals (Figs 3 and S13). These results show the scaling-up potential of the iIMAGE method and suggest that it could be used to exfoliate cheap and abundant raw materials or natural minerals to produce high-quality 2D materials.

CONCLUSION

We have developed a powerful iIMAGE method to exfoliate various layer materials into 2D materials, which is suitable for commercial-scale production. The method converts applied macroscopic compressive forces into microscopic frictional forces with the assistance of an intermediate. These forces cause slipping of the layers in the layer materials resulting in highly efficient exfoliation. Taking h-BN as an example, the iIMAGE-prepared 2D h-BN has a good quality, an average thickness of 4 nm (~12 layers), and an average lateral size of 1.2 μm. Moreover, this method has one of the highest yields, the highest production rate, the lowest energy consumption, and the best scalable production ability of all currently available techniques. The generality of this method has been proven by the effective exfoliation of several layer materials including graphite, Bi₂Te₃, b-P, MoS₂, TiO_x, h-BN, and mica, covering 2D metals, semiconductors with different bandgaps, and insulators. The scaling-up capability of the

iIMAGE technique has been demonstrated by exfoliating the cheap and abundant mineral, molybdenite, to produce 2D MoS₂ in large quantities. The iIMAGE method overcomes one of the main challenges, scalable production, in the 2D materials field, and is expected to significantly accelerate their commercialization for a wide range of applications.

METHODS

Materials

h-BN (with an average size of 30 μm, Qinhuangdao ENO High-Tech Material Development Co., Ltd., China), graphite (325 mesh, Shanghai Macklin Biochemical Co., Ltd., China), mica (600 mesh, Shandong Usolf Chemical Tech. Co., Ltd., China), MoS₂ (<2 μm, Shanghai Macklin Biochemical Co., Ltd., China), *n*-type Bi₂Te₃ (1500 mesh, Wuhan Xinrong New Materials Co., Ltd., China), molybdenite concentrate (<15 μm, collected from the Sandaozhuang open-pit mine, Luoyang, China), SiC (150 mesh, purity >97%, Dongtai Mingzhi Silicon Carbide Co., Ltd., China) and sea sand (~1 mm, collected from a local beach in Shenzhen, China) were used as-received. The synthesis of bulk TiO_x crystal is based on previous work [45] with some modifications, and the details will be published later. In short, the preparation process could be divided into two stages, including (i) alkali metal ion intercalation and (ii) protonation of the titanates. In stage (i), the layered K_{0.8}Ti_{1.73}Li_{0.27}O₄ was prepared by grinding and heating a stoichiometric mixture of

TiO₂, K₂CO₃, and Li₂CO₃ at 1000 °C for two times. After the first calcination for 5 h, the intermediate products need to be taken out and ground, followed by the second calcination for 20 h. In stage (ii), the stage (i) obtained K_{0.8}Ti_{1.73}Li_{0.27}O₄ (1 g) was added into HCl solution (1 M, 200 mL) and stirred for 4 d continuously. After stopping stirring, the product H_{1.07}Ti_{1.73}O₄ was obtained by washing the sediment with plenty of water and drying at room temperature. Then, the H_{1.07}Ti_{1.73}O₄ bulk underwent the iMAGE exfoliation process to prepare TiO_x flakes. Bulk crystals of b-P were grown by mineralizer-assisted short-distance transport (SDT) reactions. Different liquids, including DI water (Millipore Milli-Q water purification system, 18.2 MΩ) and dimethylformamide (DMF, purity >99 wt%, Shanghai Macklin Biochemical Co., Ltd., China) were used without further purification.

Detailed procedure of the iMAGE process

In a typical process, raw h-BN particles (2 g) and force intermediates (SiC, 8 g) were added to a fast rotation apparatus (Retsch RM200, Germany), and ground for 270 min under a compressive force of around 100 newtons. To exfoliate air-stable layer materials like h-BN, graphite, Bi₂Te₃, MoS₂, TiO_x and mica, the iMAGE process was performed in ambient atmosphere. To exfoliate air-sensitive layer materials, such as b-P, the iMAGE was performed in a glove box (500 × 600 × 600 mm³), which was evacuated and then filled with argon or nitrogen gas twice before the exfoliation process. For large-scale exfoliation, a molybdenite concentrate (15 g) and SiC (20 g) were ground together for 270 min under ambient atmosphere.

The as-ground mixture was added to liquids (DMF for b-P and water for the others). After standing for 8 h, a sediment was clearly seen at the bottom of the container, and the exfoliated 2D materials were stably dispersed in the supernatant. To collect the exfoliated 2D materials from the supernatant, the dispersion was centrifuged at 1500 rpm for 30 min, and then vacuum filtered onto an alumina membrane with a pore size of 20 nm.

Material characterization

A UV-vis-NIR absorption spectrometer (Agilent Cary 5000, USA) was used to characterize the exfoliated 2D materials in dispersion. Optical microscopy (Carl Zeiss Axio Imager 2, Germany), AFM (tapping mode, Oxford Instruments, UK), SEM (Hitachi SU8010, 15 kV, Japan), TEM (FEI Tecnai G2 F30, 300 kV, USA) and a laser particle size

analyzer (Malvern Zetasizer Nano-ZS90, UK) were used to characterize the morphology and structure of the exfoliated 2D materials, including their lateral size, thickness, crystal quality, etc. Raman spectroscopy (514 nm laser with a power density of 1 mW cm⁻², Horiba LabRAM ER, Japan) was used to examine the quality of the bulk and exfoliated 2D materials. XPS (monochromatic Al Kα X-rays, 1486.6 eV, PHI VersaProbe II, Japan) and FTIR (Thermo Scientific Nicolet iS 50, USA) were used to examine the chemistry of the bulk and exfoliated 2D h-BN. In addition, XPS and powder XRD (with monochromatic Cu Kα radiation λ = 0.15418 nm, Bruker D8 Advance, Germany) were used to examine the purity and crystallinity of the exfoliated 2D materials collected from the supernatant.

SUPPLEMENTARY DATA

Supplementary data are available at [NSR](#) online.

ACKNOWLEDGEMENTS

We thank Mingqiang Liu for the growth of bulk b-P crystals by the short-distance transport method, Dr. Peng Wang from the Luoyang Shenyu Molybdenum Co., Ltd. for providing raw MoS₂ and molybdenite concentrate from the Sandaozhuang open-pit mine, and Profs. Feiyu Kang and Jingyu Xu for helpful discussions. We also thank the Development and Reform Commission of Shenzhen Municipality for the development of the 'Low-Dimensional Materials and Devices' discipline.

FUNDING

This work was supported by the National Natural Science Foundation of China (51722206, 51920105002 and 51521091), the Bureau of Industry and Information Technology of Shenzhen for the '2017 Graphene Manufacturing Innovation Center Project' (201901171523), the Youth 1000-Talent Program of China, and the Guangdong Innovative and Entrepreneurial Research Team Program (2017ZT07C341).

AUTHOR CONTRIBUTIONS

B.L. and H.M.C. conceived the idea and supervised the project. C.Z., J.T., and Y.P. performed most materials exfoliation and characterization experiments. C.Z., J.T., X.C., X.Z., B.L., and H.M.C. analyzed the results. C.Z., J.T., X.C., B.L., and H.M.C. wrote the manuscript with feedback from the other authors.

Conflict of interest statement. None declared.

REFERENCES

1. Cai X, Luo Y and Liu B *et al.* Preparation of 2D material dispersions and their applications. *Chem Soc Rev* 2018; **47**: 6224–66.

2. Anasori B, Lukatskaya MR and Gogotsi Y. 2D metal carbides and nitrides (MXenes) for energy storage. *Nat Rev Mater* 2017; **2**: 16098.
3. Zhu Y, Murali S and Stoller MD *et al*. Carbon-based supercapacitors produced by activation of graphene. *Science* 2011; **332**: 1537–41.
4. Li D, Muller MB and Gilje S *et al*. Processable aqueous dispersions of graphene nanosheets. *Nat Nanotechnol* 2008; **3**: 101–5.
5. Zhu Y, Ji H and Cheng HM *et al*. Mass production and industrial applications of graphene materials. *Natl Sci. Rev* 2018; **5**: 90–101.
6. Watts MC, Picco L and Russell-Pavier FS *et al*. Production of phosphorene nanoribbons. *Nature* 2019; **568**: 216–20.
7. Mounet N, Gibertini M and Schwaller P *et al*. Two-dimensional materials from high-throughput computational exfoliation of experimentally known compounds. *Nat Nanotechnol* 2018; **13**: 246–52.
8. Wu T, Zhang X and Yuan Q *et al*. Fast growth of inch-sized single-crystalline graphene from a controlled single nucleus on Cu-Ni alloys. *Nat Mater* 2016; **15**: 43–7.
9. Fan Z, Huang X and Han Y *et al*. Surface modification-induced phase transformation of hexagonal close-packed gold square sheets. *Nat Commun* 2015; **6**: 6571.
10. Wang XY, Narita A and Muellen K. Precision synthesis versus bulk-scale fabrication of graphenes. *Nat Rev Chem* 2017; **2**: 1–10.
11. Ren W and Cheng HM. The global growth of graphene. *Nat Nanotechnol* 2014; **9**: 726–30.
12. Luo Y, Tang L and Khan U *et al*. Morphology and surface chemistry engineering toward pH-universal catalysts for hydrogen evolution at high current density. *Nat Commun* 2019; **10**: 269.
13. Sun Z, Liao T and Dou Y *et al*. Generalized self-assembly of scalable two-dimensional transition metal oxide nanosheets. *Nat Commun* 2014; **5**: 3813.
14. Tian B, Tian B and Smith B *et al*. Facile bottom-up synthesis of partially oxidized black phosphorus nanosheets as metal-free photocatalyst for hydrogen evolution. *Proc Natl Acad Sci USA* 2018; **115**: 4345–50.
15. Eda G and Chhowalla M. Chemically derived graphene oxide: towards large-area thin-film electronics and optoelectronics. *Adv Mater* 2010; **22**: 2392–415.
16. Coleman JN, Lotya M and O'Neill A *et al*. Two-dimensional nanosheets produced by liquid exfoliation of layered materials. *Science* 2011; **331**: 568–71.
17. Lei W, Mochalin VN and Liu D *et al*. Boron nitride colloidal solutions, ultralight aerogels and freestanding membranes through one-step exfoliation and functionalization. *Nat Commun* 2015; **6**: 8849.
18. Zeng Z, Sun T and Zhu J *et al*. An effective method for the fabrication of few-layer-thick inorganic nanosheets. *Angew Chem Int Ed* 2012; **51**: 9052–6.
19. Novoselov KS, Geim AK and Morozov SV *et al*. Electric field effect in atomically thin carbon films. *Science* 2004; **306**: 666–9.
20. Zhu W, Gao X and Li Q *et al*. Controlled gas exfoliation of boron nitride into few-layered nanosheets. *Angew Chem Int Ed* 2016; **55**: 10766–70.
21. Chen S, Xu R and Liu J *et al*. Simultaneous production and functionalization of boron nitride nanosheets by sugar-assisted mechanochemical exfoliation. *Adv Mater* 2019; **31**: 1804810.
22. Paton KR, Varrla E and Backes C *et al*. Scalable production of large quantities of defect-free few-layer graphene by shear exfoliation in liquids. *Nat Mater* 2014; **13**: 624–30.
23. Blake P, Brimicombe PD and Nair RR *et al*. Graphene-based liquid crystal device. *Nano Lett* 2008; **8**: 1704–8.
24. Varrla E, Paton KR and Backes C *et al*. Turbulence-assisted shear exfoliation of graphene using household detergent and a kitchen blender. *Nanoscale* 2014; **6**: 11810–9.
25. Bonaccorso F, Bartolotta A and Coleman JN *et al*. 2D-crystal-based functional inks. *Adv Mater* 2016; **28**: 6136–66.
26. Scharf TW and Prasad SV. Solid lubricants: a review. *J Mater Sci* 2013; **48**: 511–31.
27. Prasad SV and Zabinski JS. Tribology of tungsten disulphide (WS₂): characterization of wear-induced transfer films. *J Mater Sci Lett* 1993; **12**: 1413–5.
28. Wang W, Dai S and Li X *et al*. Measurement of the cleavage energy of graphite. *Nat Commun* 2015; **6**: 7853.
29. Björkman T, Gulans A and Krashennnikov AV *et al*. Van der Waals bonding in layered compounds from advanced density-functional first-principles calculations. *Phys Rev Lett* 2012; **108**: 235502.
30. Li X, Hao X and Zhao M *et al*. Exfoliation of hexagonal boron nitride by molten hydroxides. *Adv Mater* 2013; **25**: 2200–4.
31. Lee D, Lee B and Park KH *et al*. Scalable exfoliation process for highly soluble boron nitride nanoplatelets by hydroxide-assisted ball milling. *Nano Lett* 2015; **15**: 1238–44.
32. Weng Q, Kvashnin DG and Wang X *et al*. Tuning of the optical, electronic, and magnetic properties of boron nitride nanosheets with oxygen doping and functionalization. *Adv Mater* 2017; **29**: 1700659.
33. Voiry D, Mohite A and Chhowalla M. Phase engineering of transition metal dichalcogenides. *Chem Soc Rev* 2015; **44**: 2702–12.
34. Tang DM, Kvashnin DG and Najmaei S *et al*. Nanomechanical cleavage of molybdenum disulphide atomic layers. *Nat Commun* 2014; **5**: 3631.
35. Du M, Wu Y and Hao X *et al*. A facile chemical exfoliation method to obtain large size boron nitride nanosheets. *CrystEngComm* 2013; **15**: 1782–6.
36. Nair RR, Blake P and Grigorenko AN *et al*. Fine structure constant defines visual transparency of graphene. *Science* 2008; **320**: 1308.
37. Kim KS, Zhao Y and Jang H *et al*. Large-scale pattern growth of graphene films for stretchable transparent electrodes. *Nature* 2009; **457**: 706–10.
38. Osada M, Yoguchi S and Itose M *et al*. Controlled doping of semiconducting titania nanosheets for tailored spinelectronic materials. *Nanoscale* 2014; **6**: 14227–36.
39. Pan XF, Gao HL and Lu Y *et al*. Transforming ground mica into high-performance biomimetic polymeric mica film. *Nat Commun* 2018; **9**: 2974.
40. Srivastava P and Singh K. Low temperature reduction route to synthesise bismuth telluride (Bi₂Te₃) nanoparticles: structural and optical studies. *J Exp Nanosci* 2014; **9**: 1064–74.
41. Zhao W, Ghorannevis Z and Amara KK *et al*. Lattice dynamics in mono- and few-layer sheets of WS₂ and WSe₂. *Nanoscale* 2013; **5**: 9677–83.
42. Backes C, Smith RJ and McEvoy N *et al*. Edge and confinement effects allow in situ measurement of size and thickness of liquid-exfoliated nanosheets. *Nat Commun* 2014; **5**: 4576.
43. Woomer AH, Farnsworth TW and Hu J *et al*. Phosphorene: synthesis, scale-up, and quantitative optical spectroscopy. *ACS Nano* 2015; **9**: 8869–84.
44. Hanlon D, Backes C and Doherty E *et al*. Liquid exfoliation of solvent-stabilized few-layer black phosphorus for applications beyond electronics. *Nat Commun* 2015; **6**: 8563.
45. Sasaki T, Kooli F and Lida M *et al*. A mixed alkali metal titanate with the lepidocrocite-like layered structure. Preparation, crystal structure, protonic form, and acid-base intercalation properties. *Chem Mater* 1998; **10**: 4123–8.